

A note on fitting a generalized Moody diagram for wall modeled Large Eddy Simulations

Charles Meneveau^a

Department of Mechanical Engineering and Center for Environmental and Applied Fluid Mechanics, Johns Hopkins University, Baltimore MD 21218, USA.

ARTICLE HISTORY

Compiled June 20, 2022

ABSTRACT

Motivated by the needs of wall modeled Large Eddy Simulation (LES), we introduce fits to numerical solutions of the Reynolds Averaged Navier Stokes equations in their near-wall, boundary layer approximation including a mixing-length model. We provide practical fits that encompass a smooth transition between the viscous sublayer and inertial logarithmic layer, and include moderate pressure gradients as well as roughness effects. The proposed generalized fit function complies with analytical solutions valid in various asymptotic regimes and obviates the need for numerical iterative solution methods or numerical integration of ordinary differential equations during LES.

KEYWORDS

Turbulence, Wall Model, Large Eddy Simulations

1. Introduction

Wall-resolving Large-Eddy-Simulation (LES) of high Reynolds number wall-bounded flows continues to be a challenge due largely to stringent near wall resolution requirements. A large number of grid points is required to resolve the inner, viscous dominated region, and that number increases rapidly with Reynolds number. Conversely, wall modeled LES exhibits a much weaker dependence on Reynolds number and is therefore a necessary choice when applying LES to high Reynolds number wall-bounded flows. A variety of wall models have been developed for LES and reviews of many of them can be found in Refs. [1–3]. The most frequently used wall model is the so-called equilibrium wall model. There are typically three most commonly used approaches to implement the equilibrium wall model, each valid in different Reynolds number ranges and types of surfaces. (a) The rough-wall, high Reynolds number wall model, used e.g. in [4–6]. The approach assumes that the streamwise mean velocity profile in a direction normal to the surface (coordinate y) is given by $\langle u_s(y) \rangle = (u_\tau/\kappa) \log(y/z_0)$. Here z_0 is the roughness length. Evaluating this expression at a distance $y = \Delta_y$ where the streamwise velocity is known from LES (denoted as $U_{LES} = \langle u_s(\Delta_y) \rangle$) allows one to directly solve for u_τ as function of U_{LES} , Δ_y , κ and z_0 . The assumption is that Δ_y falls in the logarithmic layer and that κ is known (e.g. $\kappa = 0.4$). (b) The smooth surface case at finite Reynolds number: For flow over smooth surfaces, the equilibrium wall

^ameneveau@jhu.edu

model approach is based on the assumed profile $\langle u_s(y) \rangle = u_\tau [\kappa^{-1} \log(yu_\tau/\nu) + B]$. This now yields a transcendental equation for u_τ which must be solved iteratively in a code. Specifically, one solves $U_{\text{LES}} = u_\tau [0.4^{-1} \log(\Delta_y u_\tau/\nu) + 5]$ for u_τ , for given U_{LES} , Δ_y and ν . Again, this method assumes Δ_y falls in the logarithmic layer. If Δ_y falls in the viscous sublayer one must instead assume a linear profile [7], or one can use a smooth fit to the entire profile such as the classic fit by Reichardt (1951) [8] or the recent work in Refs. [9,10] including pressure gradient effects. Typically the fitted solution is for the velocity profile in inner units, which means that further iterative methods are needed to find the friction velocity. (c) Numerical integration of an ordinary differential equation (ODE method): Typically, if one wishes to ensure a smooth transition between the viscous and log-layer regions, to include additional physical effects, or to apply the approach to other variables such as temperature, a common approach is to use numerical solution of an ODE [3]. For the case of an equilibrium layer the ODE to be solved for the streamwise velocity reads

$$\frac{d}{dy} \left((\nu + \nu_T) \frac{d\langle u_s(y) \rangle}{dy} \right) = 0, \quad (1)$$

subject to boundary conditions $\langle u_s(0) \rangle = 0$ and $\langle u_s(\Delta_y) \rangle = U_{\text{LES}}$. The turbulent eddy viscosity ν_T can be prescribed using a mixing length model including a van-Driest damping function.

It would appear useful to cast the solution of this sort of ODE into a general form, solve it numerically once and for all, and to provide useful fits to the (inverse) solution that can be applied uniformly to a large number of LES cases. One reason that many researchers opt for numerical solution is that the ODE itself depends upon the unknown dimensional parameter u_τ via the van-Driest damping function and that when written in inner units as function of y^+ the equation must be integrated numerically up to a case-dependent position $y^+ = \Delta^+$ which itself depends on the unknown value of u_τ . We shall address this issue by rewriting the equation in a non-standard dimensionless form in terms of two Reynolds numbers that facilitates generalization for wall modeling. Another reason researchers opt for numerical solution of the boundary layer equation is that it is then possible to include additional physical effects such as pressure gradient, which we shall address here, or handle other fields such as temperature, which we will not address.

The aims of this note are thus rather modest, namely to reformulate Eq. 1 in such a way as to facilitate numerical integration and fitting of the results in the context of wall-modeled LES (WMLES). Specifically, we fit the *inverse* of the solution to the velocity profile, i.e. we will be able to find $u_\tau = f(\text{known variables})$ directly using relatively simple function evaluations. We also aim to include (moderate) pressure gradient effects and to merge the resulting fits smoothly to the equilibrium wall model approach valid for rough-wall, high Reynolds number boundary layers. This note does not include implementation and applications in LES codes, but documents errors and differences between the proposed fits and the full numerical solution of the corresponding ODE (RANS) equations. Also, we do not address any of the other fundamental issues underlying wall modeling using the equilibrium wall model, such as the log-layer mismatch and challenges associated with modeling non-equilibrium unsteady terms, issues treated e.g. in Refs. [7,11–13].

It is hoped that the generalized fits provided (a kind of “generalized Moody diagram” for wall modeling) can save computational resources and simplify implementations of equilibrium wall models in LES.

2. Determining the wall stress in terms of known velocity:

We first focus on the simplest case of wall modeling in which we consider only the streamwise direction (subscripts “s”) without pressure gradient or other acceleration terms. We assume the streamwise velocity away from the wall is known, and denote it by $U_{\text{LES}} = \langle u_s(\Delta_y) \rangle$. The unknown to be determined is the friction velocity u_τ , from which the (kinematic) wall stress in the streamwise direction can then be evaluated according to $\tau_w = u_\tau^2$ and oriented according to the usual approaches [1–3,6]. To cast the problem into a dimensionless framework, we now define two Reynolds numbers:

$$Re_\Delta = \frac{U_{\text{LES}}\Delta_y}{\nu} \quad \text{and} \quad Re_{\tau\Delta} = \frac{u_\tau\Delta_y}{\nu}. \quad (2)$$

In WMLES, Re_Δ is the known input whereas $Re_{\tau\Delta} = \Delta_y^+$ is the unknown output for which we wish to solve and then obtain u_τ .

Using the usual mixing length model, integrating Eq. 1 once and using the fact that the stress tends to u_τ^2 as $y \rightarrow 0$ we have

$$\left(\nu + [D(y)\kappa y]^2 \left| \frac{du}{dy} \right| \right) \frac{du}{dy} = u_\tau^2, \quad (3)$$

where for notational simplicity henceforth we set $u = \langle u_s \rangle$. The traditional van Driest damping function is included: $D(y) = [1 - \exp(-y^+/A^+)]$ with $y^+ = (y/\Delta_y)Re_{\tau\Delta}$, and $A^+ = 25$ is a commonly used value.

We first develop a numerical integration by recasting this equation in terms of dimensionless variables that can be expressed in terms of the dimensional parameters known in LES (besides U_{LES}), namely Δ_y and ν :

$$y' = \frac{y}{\Delta_y}, \quad \hat{u}(y') = \frac{u(y)\Delta}{\nu}. \quad (4)$$

The equation then reads as follows:

$$\frac{d\hat{u}}{dy'} + [D(y')\kappa y']^2 \left(\frac{d\hat{u}}{dy'} \right)^2 = Re_{\tau\Delta}^2 \quad (5)$$

(we assume a monotonic profile, where du/dy does not change sign). Solving the quadratic equation [14] casts it into a simple first-order ODE for $\hat{u}(y')$:

$$\frac{d\hat{u}}{dy'} = \frac{1}{2[D(y')\kappa y']^2} \left(-1 + \sqrt{1 + 4[D(y')\kappa y']^2 Re_{\tau\Delta}^2} \right), \quad (6)$$

where $D(y') = 1 - \exp(-y'Re_{\tau\Delta}/25)$ and with a single boundary condition $\hat{u}(0) = 0$. Since $D(0) = 0$, the equation cannot be initialized exactly at $y' = 0$. Instead, we initialize at $y_i^+ = 10^{-3}$ or $y_i' = 10^{-3}Re_{\tau\Delta}^{-1}$. The corresponding value of $\hat{u}(y_i')$ is obtained from the near wall behavior $u(y) = (u_\tau^2/\nu)y$ or $\hat{u}(y_i') = Re_{\tau\Delta}^2 y_i'$. The integration is done numerically (Matlab ODE45), for a wide range of given $Re_{\tau\Delta}$, between 10^{-1} and 10^6 . The ‘forward’ integration is done until $y' = 1$ is reached. The value obtained as a result, $\hat{u}(1)$, corresponds to the LES velocity normalized by Δ and ν . That is to say, we find $Re_\Delta = \hat{u}(1)$ as a result of the numerical integration. Note that this approach

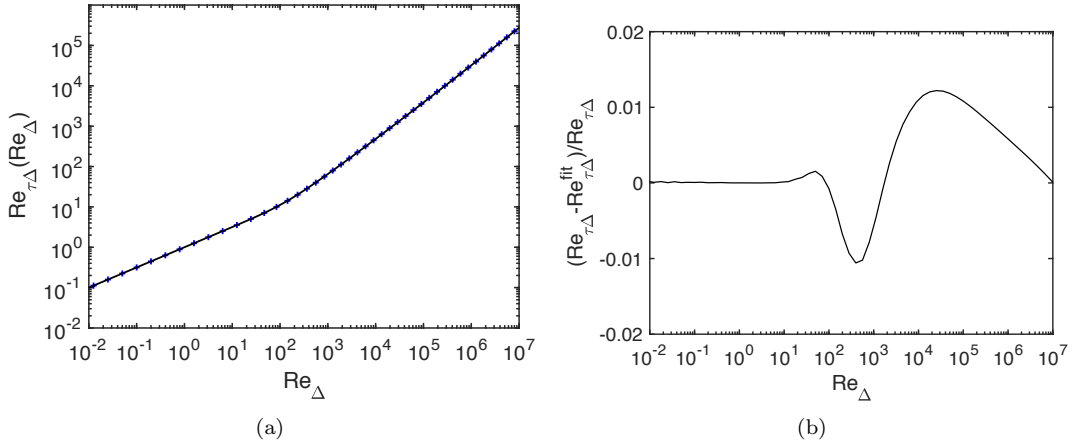


Figure 1. (a) Blue crosses: numerical solution of Eq. 6 over wide range of conditions. Dark solid line: empirical fit given by Eq. 7 with parameters given by Eqs. 8. (b) Relative error between numerical solution of Eq. 6 and empirical fit given by Eq. 7.

is equivalent to expressing the ODE in terms of y^+ and then integrating from $y^+ = 0$ up to $y^+ = Re_{\tau\Delta}$, where $Re_{\tau\Delta}$ can again be prescribed.

The results of the numerical integration are shown as symbols in Fig. 1(a). The resulting Re_{Δ} is plotted on the x-axis and the (imposed) parameter $Re_{\tau\Delta}$ on the y-axis. At small Reynolds numbers, the expected trend is $Re_{\tau\Delta} \sim Re_{\Delta}^{1/2}$ (Δ_y in viscous region), whereas at high Re_{Δ} the behavior is a slow approach to a linear behavior, with sub-leading logarithmic corrections (from the inverse log-law).

Next, we aim to fit the numerical result using an empirical function. The fit function should transition smoothly between a $1/2$ power law at low Re_{Δ} towards a power law with exponent β_1 that is on the order of 0.8-1.0 at high Re_{Δ} , and which itself can be chosen to depend upon Re_{Δ} . We use the approach proposed by Batchelor [15] in the context of structure function transitions:

$$Re_{\tau\Delta}^{\text{fit}}(Re_{\Delta}) = \kappa_4 Re_{\Delta}^{\beta_1} \left[1 + (\kappa_3 Re_{\Delta})^{-\beta_2} \right]^{(\beta_1 - 1/2)/\beta_2}. \quad (7)$$

The transition sharpness is controlled by a parameter β_2 . Choosing constant values $\beta_1 = 0.9$, $\beta_2 = 1.2$, $\kappa_3 = 0.005$, and $\kappa_4 = \kappa_3^{\beta_1 - 1/2}$ gives results with errors of around 5%. Making some of the parameters dependent on Re_{Δ} leads to improved accuracy. Specifically, we choose $\kappa_3 = 0.005$, $\kappa_4 = \kappa_3^{\beta_1 - 1/2}$, and

$$\beta_1(Re_{\Delta}) = (1 + 0.155 Re_{\Delta}^{-0.03})^{-1}, \quad \beta_2(Re_{\Delta}) = 1.7 - (1 + 36 Re_{\Delta}^{-0.75})^{-1}. \quad (8)$$

The fit is shown as solid line in Fig. 1(a), showing excellent agreement with the numerical solution over many decades. The relative error is plotted in Fig. 1(b). The errors for $0 < Re_{\Delta} < 10^7$ (which should easily cover all practical applications of WMLES) are below 1.2%.

In WMLES, for a given velocity U_{LES} , one evaluates Re_{Δ} then applies Eq. 7 and determines the friction velocity according to

$$u_{\tau} = Re_{\tau\Delta}^{\text{fit}}(Re_{\Delta}) \times \frac{\nu}{\Delta_y} = U_{\text{LES}} \frac{Re_{\tau\Delta}^{\text{fit}}}{Re_{\Delta}}. \quad (9)$$

Thus, Eq. 7 constitutes an equilibrium wall model that smoothly merges with the viscous behavior and does not require iteratively solving for u_τ or numerically integrating an ODE. It does not, however, include effects of pressure gradients, considered in the next section.

3. Effects of (mild) pressure gradient

Defining the streamwise pressure gradient term available from LES as $N = \rho^{-1} \partial \tilde{p}_{\text{LES}} / \partial s$, and again considering the momentum equation written with eddy viscosity and integrating once, yields

$$\left(\nu + (D(y)\kappa y)^2 \left| \frac{du}{dy} \right| \right) \frac{du}{dy} = Ny + u_\tau^2, \quad (10)$$

where the boundary condition that the stress tend to u_τ^2 as $y \rightarrow 0$ has been used again. We neglect the effects of pressure gradient on the eddy viscosity (see Ref. [16] as a study where such effects are included). For a favorable pressure gradient ($N < 0$), for there to be no sign changes in the slope of the velocity profile between the wall and $y = \Delta_y$, the following must hold:

$$|N| < \frac{u_\tau^2}{\Delta_y}. \quad (11)$$

The normalized equation, after solving again the quadratic equation, reads:

$$\frac{d\hat{u}}{dy'} = \frac{1}{2[D(y')\kappa y']^2} \left(-1 + \sqrt{1 + 4[D(y')\kappa y']^2 Re_{\tau\Delta}^2 (1 + \chi y')} \right), \quad (12)$$

where we have defined the pressure gradient parameter according to

$$\chi = \frac{N\Delta}{u_\tau^2} \quad (13)$$

and it is understood that the developments below require $|\chi| < 1$. The boundary condition is, again, $\hat{u}(0) = 0$. We initialize at $y_i^+ = 10^{-3}$ or $y_i' = 10^{-3} Re_{\tau\Delta}^{-1}$. The corresponding value of $\hat{u}(y_i')$ can be obtained from the quadratic expansion near the origin now including pressure gradient:

$$u(y) = \frac{u_\tau^2}{\nu} y + \frac{N}{2\nu} y^2 + \dots, \quad \text{or} \quad \hat{u}(y_i') = Re_{\tau\Delta}^2 \left(y_i' + \frac{1}{2} \chi y_i'^2 + \dots \right) \quad (14)$$

The integration is done again numerically (Matlab ODE45) and we obtain $Re_\Delta = \hat{u}(1)$. The operation is repeated for a range of values of $Re_{\tau\Delta}$ and χ . The results are shown using symbols in Fig. 4. The effect of pressure gradient can be more readily appreciated by comparing to the $\chi = 0$ case, by plotting the ratio $Re_{\tau\Delta}(Re_\Delta, \chi) / Re_{\tau\Delta}(Re_\Delta, 0)$, shown in Fig. 3(a)

In order to “invert” these results we again propose an empirical fit that will now also depend on χ . We note that $\chi = N\Delta/u_\tau^2$, and since u_τ is not known a-priori, χ

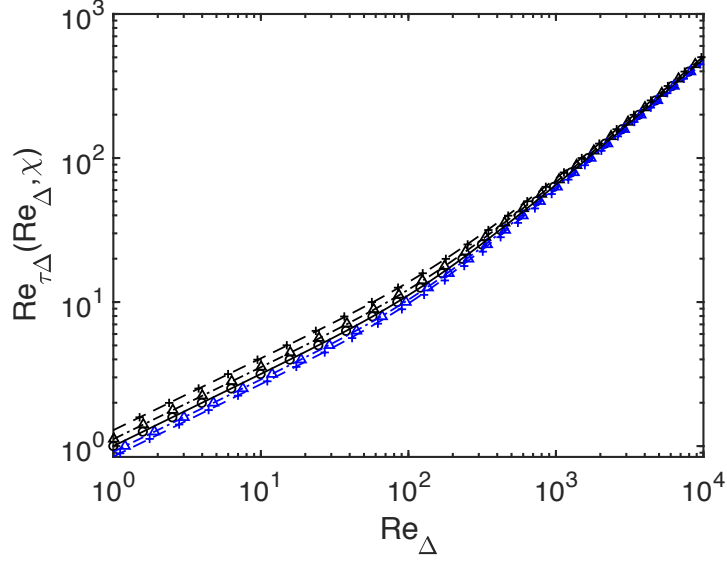


Figure 2. Symbols: numerical solution of Eq. 12 over a range of Reynolds numbers $Re_{\tau\Delta}$, for $\chi = -0.8$ (black +), $\chi = -0.4$ (black triangles), $\chi = 0$ (circles), $\chi = -0.4$ (blue triangles), $\chi = -0.8$ (blue +). Only the region between $1 < Re_{\Delta} < 10^4$ is shown for clarity. Lines: empirical fit given by Eqs. 26 and 25. Solid line: $\chi = 0$, dot-dashed lines: $|\chi| = 0.4$, dashed line: $|\chi| = 0.8$. Black: favorable pressure gradient ($\chi \leq 0$), blue lines: adverse pressure gradient $\chi > 0$.

cannot be directly evaluated in LES. However since the effect of χ on $Re_{\tau\Delta}$ is relatively weak, in LES we may evaluate χ using

$$\chi \approx \frac{N\Delta}{u_{\tau 0}^2}, \quad (15)$$

where $u_{\tau 0}$ is based on U_{LES} only, i.e. $u_{\tau 0} = U_{LES} Re_{\tau\Delta}^{\text{fit}}(Re_{\Delta})/Re_{\Delta}$, using the fit of Eq. 7 that assumes $\chi = 0$ as a first guess:

$$\chi \approx \frac{N\Delta}{U_{LES}^2} \left(\frac{Re_{\Delta}}{Re_{\tau\Delta}^{\text{fit}}(Re_{\Delta})} \right)^2. \quad (16)$$

In order to develop fits to the dependence of $Re_{\tau\Delta}$ on Re_{Δ} for $\chi \neq 0$, it is instructive to consider the two asymptotic limits at low and high Re_{Δ} . In the viscous range (i.e. if $Re_{\tau\Delta} \ll 10$) we can obtain from Eq. 14 (using $y' = 1$):

$$Re_{\Delta} = Re_{\tau\Delta}^2 \left(1 + \frac{1}{2}\chi \right). \quad (17)$$

But also, $Re_{\Delta} = Re_{\tau\Delta}^2(\chi = 0)$, i.e. the value for $\chi = 0$. We may obtain $Re_{\tau\Delta}$ via the baseline fit in Eq. 7 for $\chi = 0$ at small Re_{Δ} . Hence we write as the viscous limiting behavior:

$$Re_{\tau\Delta,v} = Re_{\tau\Delta}(\chi = 0) \left(1 + \frac{1}{2}\chi \right)^{-1/2} = Re_{\tau\Delta}^{\text{fit}}(Re_{\Delta}) \left(1 + \frac{1}{2}\chi \right)^{-1/2}. \quad (18)$$

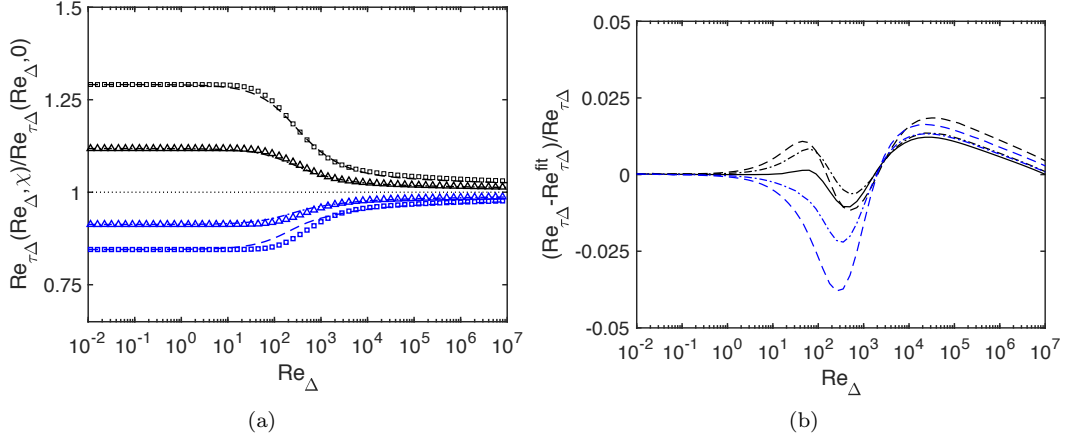


Figure 3. (a) Symbols: Ratio of friction Reynolds number as function Re_{Δ} obtained from numerical integration, for: $\chi = -0.8$ (black squares), $\chi = -0.4$ (black triangles), $\chi = -0.4$ (blue triangles), $\chi = -0.8$ (blue squares). The relative effect of pressure gradient is larger at lower Reynolds number. The lines are from an empirical fit (Eqs. 26,25). (b) Relative error between numerical solution of Eq. 12 and empirical fit given by Eqs. 26 and 25. Solid line: $\chi = 0$, dot-dashed lines: $|\chi| = 0.4$, dashed line: $|\chi| = 0.8$. Black: favorable pressure gradient ($\chi \leq 0$), blue lines: adverse pressure gradient $\chi > 0$.

Next, we consider the limiting behavior of the solution in the inertial layer far above the viscous region, i.e. when viscosity can be neglected. The ODE simplifies to

$$\frac{d\hat{u}}{dy'} = \frac{Re_{\tau\Delta}}{\kappa y'} \sqrt{1 + \chi y'} \approx Re_{\tau\Delta} \left(\frac{1}{\kappa y'} + \frac{1}{2\kappa} \chi \right). \quad (19)$$

where we have made the further assumption that $|\chi| \ll 1$ so that $\sqrt{1 + \chi y'} \approx 1 + \frac{1}{2}\chi y'$. Integration yields

$$\hat{u}(y') = Re_{\tau\Delta} \left(\frac{1}{\kappa} \log y' + \frac{1}{2\kappa} \chi y' + C_1 \right). \quad (20)$$

Interestingly, and consistent with the Ansatz used in the integral wall model (iWM-LES) of Ref. [7], pressure gradient effects are seen to add a linear term to the profile. Using the condition that $\hat{u}(1) = U_{LES}\Delta/\nu = Re_{\Delta}$ yields

$$\hat{u}(y') = Re_{\Delta} - Re_{\tau\Delta} \left(\frac{1}{\kappa} \log(1/y') + \frac{1}{2\kappa} \chi(1 - y') \right). \quad (21)$$

We recall that this assumes that Δ_y is in the log-region, since molecular viscosity has been neglected. Hence, $Re_{\tau\Delta} \gg 30$ is assumed. Another condition must be invoked to determine $Re_{\tau\Delta}$ given a value of Re_{Δ} . Specifically we match with the viscous behavior

$$\hat{u}(y') = Re_{\tau\Delta}^2 y', \quad (22)$$

at $y^+ = 11$ or $y' = 11/Re_{\tau\Delta}$. We note that inclusion of the pressure gradient affected second-order term and matching at the height suggested by Nickels [17] yields only a negligible corrections, and will be neglected. Isolating Re_{Δ} and using the fact that

$11 - \kappa^{-1} \log(11) = B$ for $\kappa = 0.4$ and $B = 5$, we obtain

$$Re_{\Delta} = Re_{\tau\Delta} \left(\frac{1}{\kappa} \log Re_{\tau\Delta} + B + \frac{1}{2\kappa} \chi (1 - 11/Re_{\tau\Delta}) \right). \quad (23)$$

We remark that since $Re_{\Delta}/Re_{\tau\Delta} = u^+(y = \Delta_y)$, the above result shows that as $Re_{\tau\Delta} \gg 11$, the effect of pressure gradient becomes an offset similar to B , i.e. $B' = B + \chi/(2\kappa)$. For favorable pressure gradient ($\chi < 0$), there is a downward shift indicating a larger stress for a given velocity (the profile is steeper near the wall) and vice versa. Since $2\kappa \sim O(1)$, the velocity shift due to pressure gradients is about $\sim \pm u_{\tau}$ for $|\chi| \sim 1$.

Moreover, we can use this expression to deduce the asymptotic behavior at large $Re_{\tau\Delta}$ by using the already developed fit $Re_{\tau\Delta}^{\text{fit}}(Re_{\Delta})$ as follows. Rewrite Eq. 23 as

$$Re_{\Delta}^* \equiv Re_{\Delta} - Re_{\tau\Delta} \frac{1}{2\kappa} \chi (1 - 11/Re_{\tau\Delta}) = Re_{\tau\Delta} \left(\frac{1}{\kappa} \log Re_{\tau\Delta} + B \right). \quad (24)$$

When applied to the logarithmic layer at large $Re_{\tau\Delta}$, the fitting formula Eq. 7 can be regarded as inverting the log-law. It can now be applied in the inertial layer according to Eq. 24 to solve for $Re_{\tau\Delta}$ for a given Re_{Δ}^* , i.e. to obtain $Re_{\tau\Delta, \text{in}} = Re_{\tau\Delta}^{\text{fit}}(Re_{\Delta}^*)$ as function of Re_{Δ}^* , where Re_{Δ}^* takes the place of Re_{Δ} in Eq. 7.

Some practical steps must now be invoked to develop a useful fitting formula. Firstly, the additive correction used to compute Re_{Δ}^* requires some adjustment to smoothly merge to zero when $Re_{\tau\Delta} < 11$. We multiply the entire additive term by a factor that tends to zero when $Re_{\tau\Delta}$ becomes smaller than $O(10)$. The following expression yields good results:

$$Re_{\Delta}^* = Re_{\Delta} - Re_{\tau\Delta}^{\text{fit}} \frac{1}{2\kappa} \chi \left(1 - \frac{11}{Re_{\tau\Delta}^{\text{fit}}} \right) \left[1 + \left(\frac{50}{Re_{\tau\Delta}^{\text{fit}}} \right)^2 \right]^{-1/2}. \quad (25)$$

Since the additive term depends upon the unknown value of $Re_{\tau\Delta}$, it has been written here in terms of the fitted value for $\chi = 0$, i.e. $Re_{\tau\Delta}^{\text{fit}}(Re_{\Delta})$ (Eq. 7). Next, we combine the viscous and inertial functions $Re_{\tau\Delta, v}$ and $Re_{\tau\Delta, \text{in}}$ using a weighting function $\theta(Re_{\Delta}) = (1 + 0.0025 Re_{\Delta})^{-1}$ according to

$$Re_{\tau\Delta}^{\text{com}}(Re_{\Delta}, \chi) = \theta(Re_{\Delta}) Re_{\tau\Delta}^{\text{fit}}(Re_{\Delta}) (1 + \chi/2)^{-1/2} + [1 - \theta(Re_{\Delta})] Re_{\tau\Delta}^{\text{fit}}(Re_{\Delta}^*). \quad (26)$$

The lines in Figs. 4 and 3(a) show the results from using $Re_{\tau\Delta}^{\text{com}}(Re_{\Delta}, \chi)$ to predict the friction Reynolds number ratio compared to the case with zero pressure gradient. The relative error is shown in Figure 3(b), for various values of χ compared to the results from the full numerical integration of the ODE. As can be seen, errors of no more than 2.5 % are incurred. For $|\chi| < 0.4$ the errors are below 1.5%.

It must be stressed that these developments and fits are only valid for small χ , $|\chi| < 1$. For very strong pressure gradient cases, the assumption of a monotonic velocity profile below $y = \Delta_y$ and a pressure-gradient independent eddy-viscosity [16] begin to fail.

4. Effects of roughness:

The ‘infinite Reynolds number limit’ of rough wall equilibrium wall modeling is based on the profile

$$u(y) = \frac{u_\tau}{\kappa} \log\left(\frac{y}{z_0}\right), \quad (27)$$

where z_0 is the surface roughness length (typically around 2-10% of protuberance heights). Evaluated at $y = \Delta_y$ it can be rewritten as the ‘infinite’ Reynolds number rough wall limit:

$$Re_{\tau\Delta}^\infty = Re_\Delta \frac{\kappa}{\log(\Delta_y/z_0)}. \quad (28)$$

In the high Reynolds number limit, the friction and LES velocities are linearly related (the stress is quadratic with U_{LES}), and in terms of the limiting behavior of the fits in Eq. 7 this would correspond to $\beta_1 \rightarrow 1$. Note that expression 27 is applicable only for $\Delta_y \gg z_0$ and that it does not include pressure gradient effects.

Inclusion of pressure gradient can be done as follows: Integrating the inertial momentum equation including the linearized pressure gradient term and imposing $u(y = \Delta) = U_{LES}$ yields:

$$u(y) = U_{LES} - u_\tau \left[\frac{1}{\kappa} \log\left(\frac{\Delta}{y}\right) + \frac{\chi}{2\kappa} \left(1 - \frac{y}{\Delta}\right) \right]. \quad (29)$$

The definition of z_0 is that $u(z_0) = 0$, and assuming the same z_0 is not affected by pressure gradient, we may use this condition to solve for u_τ for a given U_{LES} and z_0/Δ , leading to

$$Re_{\tau\Delta}^\infty(Re_\Delta, \chi, \Delta/z_0) = Re_\Delta \left[\frac{1}{\kappa} \log\left(\frac{\Delta}{z_0}\right) + \frac{\chi}{2\kappa} \left(1 - \frac{z_0}{\Delta}\right) \right]^{-1}. \quad (30)$$

As before, to evaluate χ we can use the baseline friction velocity neglecting pressure gradient, i.e.

$$u_{\tau 0} = U_{LES} \left(\frac{\kappa}{\log(\Delta_y/z_0)} \right). \quad (31)$$

for the rough wall case (same as Eq. 28). In general, to merge with the smooth wall behavior, one would pick the larger of the two friction velocity estimates, so that we now define the χ parameter as

$$\chi = \frac{N\Delta_y}{u_{\tau 0}^2}, \quad \text{where } u_{\tau 0} = U_{LES} \max \left[\frac{Re_{\tau\Delta}^{\text{fit}}}{Re_\Delta}, \frac{\kappa}{\log(\Delta_y/z_0)} \right]. \quad (32)$$

As a reminder, the modeling validity is limited to $|\chi| < 1$, so in practice the value of χ can be clipped to lie between -1 and 1.

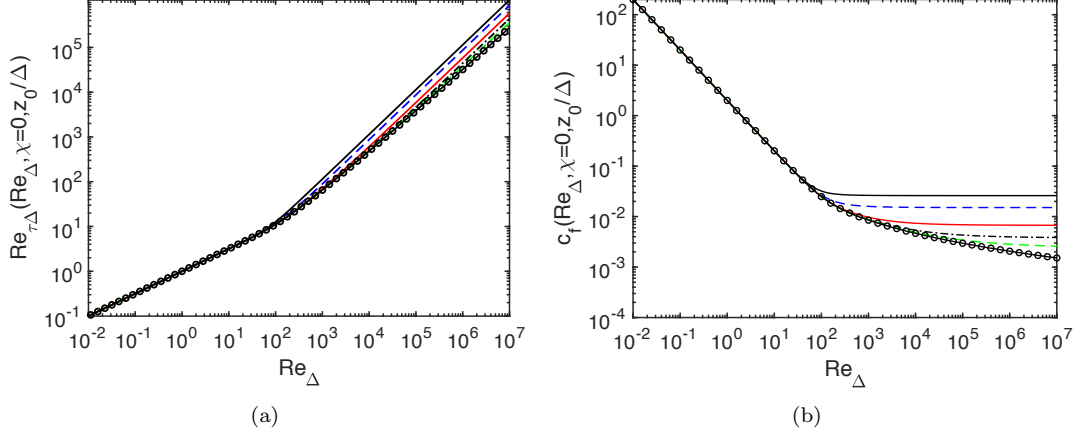


Figure 4. (a) Lines: empirical fit from the universal fitting function Eq. 33 for $\chi = 0$ for various values of roughness: $z_0/\Delta = 3 \times 10^{-2}$ (black line), $z_0/\Delta = 10^{-2}$ (blue dashed line), $z_0/\Delta = 10^{-3}$ (red line), $z_0/\Delta = 10^{-4}$ (black dot dashed line), $z_0/\Delta = 3 \times 10^{-5}$ (green dashed line), smooth surface case with $z_0/\Delta \rightarrow 0$ (circles and black line). (b) Wall model Moody diagram: Friction factor from universal fitting function for $\chi = 0$ for various values of roughness: $z_0/\Delta = 3 \times 10^{-2}$ (black line), $z_0/\Delta = 10^{-2}$ (blue dashed line), $z_0/\Delta = 10^{-3}$ (red line), $z_0/\Delta = 10^{-4}$ (black dot dashed line), $z_0/\Delta = 3 \times 10^{-5}$ (green dashed line), smooth surface case with $z_0/\Delta \rightarrow 0$ (circles and black line).

Finally, we combine the smooth and rough surface behaviors into a universal fit function with a fairly sharp transition as follows:

$$Re_{\tau\Delta}^{\text{uf}}(Re_{\Delta}, \chi, z_0/\Delta) = [Re_{\tau\Delta}^{\infty}(Re_{\Delta}, \chi, z_0/\Delta)^6 + Re_{\tau\Delta}^{\text{com}}(Re_{\Delta}, \chi)^6]^{1/6}, \quad (33)$$

where $Re_{\tau\Delta}^{\text{com}}$ is given by Eq. 26 and $Re_{\tau\Delta}^{\infty}$ by Eq. 30. Equation 33 represents the main result combining all prior effects considered in this paper.

Figure 4(a) shows the results for $\chi = 0$ for various values of the roughness parameter z_0/Δ . Figure 4(b) shows the same result expressed in terms of the more familiar friction parameter

$$c_f^{\text{wm}} = \frac{u_{\tau}^2}{\frac{1}{2}U_{\text{LES}}^2} = 2 \left(\frac{Re_{\tau\Delta}}{Re_{\Delta}} \right)^2, \quad (34)$$

resulting in a ‘generalized wall model Moody diagram’.

Another way to display the behavior of the rough-wall fit is to compute the corresponding velocity defect,

$$\Delta U^+ = \frac{U_s - U_r}{u_{\tau}} = \frac{Re_{\Delta,s}}{Re_{\tau\Delta}} - \frac{Re_{\Delta,r}}{Re_{\tau\Delta}} \quad (35)$$

where for a given value of u_{τ} , U_r is the velocity at $y = \Delta_y$ corresponding to a rough surface and U_s for a smooth surface. The sand-grain roughness in viscous units is given by the equivalency [18], valid in the fully rough regime:

$$U^+ = \frac{1}{\kappa} \log \frac{y^+}{z_0^+} = \frac{1}{\kappa} \log \frac{y^+}{k_{s,\infty}^+} + 8.5 \quad (36)$$

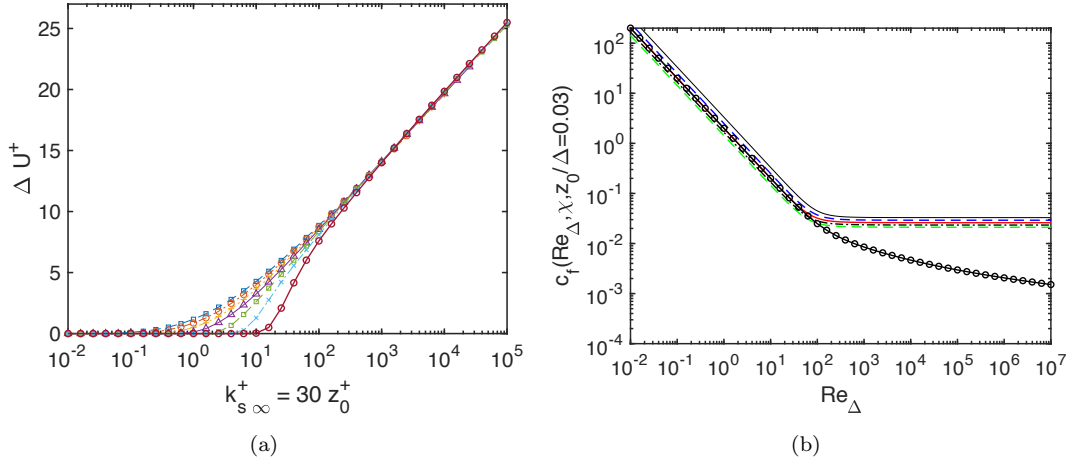


Figure 5. (a) Roughness function ΔU^+ , as function of sand-grain roughness in viscous units $k_{s,\infty}^+$, for $\chi = 0$ for various values of roughness: $z_0/\Delta = 10^{-1}$ (red circles and line), $z_0/\Delta = 3 \times 10^{-2}$ (blue crosses and dot-dashed line), $z_0/\Delta = 10^{-2}$ (green squares and dashed line), $z_0/\Delta = 3 \times 10^{-3}$ (purple triangles and line), $z_0/\Delta = 3 \times 10^{-3}$ (orange pluses and dot-dashed line), $z_0/\Delta = 3 \times 10^{-4}$ (red circles and dot-dashed line) and $z_0/\Delta = 10^{-4}$ (purple squares and dashed line). Only values for which the resulting $Re_{\Delta,s}$ for smooth surfaces is $Re_{\Delta,s} < 10^7$ (limits of fit) are shown. (b) Wall model Moody diagram for single roughness value at various pressure gradients. Universal fitting function for $Re_{\tau\Delta}$ as function of Re_Δ for $z_0/\Delta = 3 \times 10^{-2}$ for various values of χ : $\chi = -0.8$ (black line), $\chi = -0.4$ (blue dashed line), $\chi = 0$ (red line), $\chi = 0.4$ (black dot dashed line), and $\chi = 0.8$ (green dashed line), smooth surface ($z_0/\Delta \rightarrow 0$) with $\chi = 0$ (circles and black line).

which implies that

$$k_{s,\infty}^+ = z_0^+ \exp(\kappa 8.5) \approx 30 z_0^+ = 30 \frac{z_0}{\Delta} Re_{\tau\Delta}. \quad (37)$$

To find ΔU^+ , for a given $k_{s,\infty}^+$ and z_0/Δ , we first determine $Re_{\tau\Delta} = 0.0333 k_{s,\infty}^+ (\Delta/z_0)$. Then we invert the fit in Eq. 33 (using *vpasolve* from MatlabTM) to find $Re_{\Delta,r}$ for the given z_0/Δ . A second inversion is used to find $Re_{\Delta,s}$ by using the fit with $z_0/\Delta = 10^{-50}$, i.e. smooth surface. Only results for which $Re_{\Delta,s} < 10^7$ (the upper limit of accuracy for the fit 33) are plotted. Figure 5(a) displays the result (we only consider $\chi = 0$ in this comparison). Comparing with Fig. 3 of Jimenez (2004) [18], it can be seen that the fitting function provides realistic-looking predictions not only of the asymptotic behaviors at large and small $k_{s,\infty}^+$, but also for the fact that the transition becomes smoother for small z_0/Δ while it can be quite abrupt for larger z_0/Δ .

The effects of pressure gradient are significant even at high Reynolds numbers for the rough surface cases. In Fig. 5(b) the results are shown for $z_0/\Delta = 3 \times 10^{-2}$ at various values of the pressure gradient parameter χ .

5. Conclusion

For convenience the entire set of fitting functions are summarized in the appendix. They enable efficient evaluation of friction velocity and wall stress in WMLES, unifying smooth wall and rough wall behaviors, including effects of moderate pressure gradients (for which the velocity profile below the LES grid point at $y = \Delta_y$ is expected to remain monotonic), as well as smoothly merging towards the viscous sublayer. It is important to recall that the fits proposed herein are for near equilibrium conditions and

that they are based on classic mixing length RANS modeling for the expected mean velocity profile, thus inheriting the drawbacks associated with these assumptions. The fits are proposed here to facilitate and unify implementation in LES codes.

Acknowledgments

The author thanks M. Fowler, Y. Hue, G. Narasimhan, T. Zaki, J. Larsson and X.I.A. Yang for many insightful conversations and comments on the topic of wall modeling for LES. Financial support for the present work was provided by the Office of Naval Research (grant # N00014-17-1-2937) and the National Science Foundation (grant # CBET-1738918).

Appendix

For convenience, we here reproduce all of the equations required in practice to implement the wall model fits presented in this paper. With inputs U_{LES} , Δ_y and fluid viscosity ν , evaluate

$$Re_{\Delta} = \frac{U_{\text{LES}}\Delta_y}{\nu}.$$

For the simplest applications (no pressure gradient, no roughness), Eq. 7 for $Re_{\tau\Delta}^{\text{fit}}$ then provides the baseline version of the wall model.

For inclusion of pressure gradient without roughness, using $\rho^{-1}\partial p_{\text{LES}}/\partial s$, Δ_y and the baseline friction velocity from 7, evaluate χ from

$$\chi = \frac{N\Delta_y}{U_{\text{LES}}^2} \left(\frac{Re_{\Delta}}{Re_{\tau\Delta}^{\text{fit}}} \right)^2$$

and then the combined model $Re_{\tau\Delta}^{\text{com}}$ according to Eq. 26 provides the model outcome.

For inclusion of roughness in the fully rough regime, one would evaluate χ according to

$$\chi = \frac{N\Delta_y}{U_{\text{LES}}^2} \left(\frac{1}{\kappa} \log(\Delta_y/z_0) \right)^2$$

and evaluate the friction Reynolds number according to Eq. 30.

For inclusion of roughness as well as pressure gradients and viscous effects, evaluate χ using Eq. 32, rewritten as

$$\chi = \frac{N\Delta_y}{U_{\text{LES}}^2} \min \left[\frac{Re_{\Delta}}{Re_{\tau\Delta}^{\text{fit}}}, \frac{1}{\kappa} \log(\Delta_y/z_0) \right]^2.$$

To ensure validity of the fits and derivations, in practice χ may have to be clipped to fall between -1 and $+1$, i.e. use $\text{sign}(\chi) \min(|\chi|, 1)$.

Finally, determine $Re_{\tau\Delta}^{\text{uf}}$ from Eq. 33 and find the friction velocity from

$$u_\tau = U_{\text{LES}} \frac{Re_{\tau\Delta}^{\text{xyz}}}{Re_\Delta} \quad (38)$$

where $Re_{\tau\Delta}^{\text{xyz}}$ is either $Re_{\tau\Delta}^{\text{fit}}$, $Re_{\tau\Delta}^{\text{com}}$, $Re_{\tau\Delta}^\infty$, or $Re_{\tau\Delta}^{\text{uf}}$ depending on the case considered. The latter ‘universal’ fit contains all of the above special cases and can thus be implemented without having to specify cases ahead of time.

The several functions that can be evaluated according to the steps listed below as function of the dimensionless inputs Re_Δ , χ and z_0/Δ_y .

FUNCTION $Re_{\tau\Delta}^{\text{uf}} = Re_{\tau\Delta}^{\text{uf}}(Re_\Delta, \chi, z_0/\Delta)$

Check: $0 < Re_\Delta < 10^7$, $|\chi| < 1$, $0 < z_0/\Delta_y < 0.1$.

$$\begin{aligned} \beta_1 &= [1 + 0.155/Re_\Delta^{0.03}]^{-1}, & \beta_2 &= 1.7 - [1 + 36/Re_\Delta^{0.75}]^{-1}, \\ \kappa &= 0.40, & \kappa_3 &= 0.005, & \kappa_4 &= \kappa_3^{\beta_1 - 1/2}, \\ Re_{\tau\Delta}^{\text{fit}} &= \kappa_4 Re_\Delta^{\beta_1} [1 + (\kappa_3 Re_\Delta)^{-\beta_2}]^{(\beta_1 - 1/2)/\beta_2}. \end{aligned} \quad (39)$$

To include pressure gradients:

$$\begin{aligned} Re_{\tau\Delta, v} &= (1 + 0.5\chi)^{-1/2} Re_{\tau\Delta}^{\text{fit}}, \\ Re_\Delta^* &= Re_\Delta - \frac{\chi}{2\kappa} Re_{\tau\Delta}^{\text{fit}} (1 - 11/Re_{\tau\Delta}^{\text{fit}}) [1 + (50/Re_{\tau\Delta}^{\text{fit}})^2]^{-1/2}, \\ \beta_1^* &= [1 + 0.155/Re_\Delta^{*0.03}]^{-1}, & \beta_2^* &= 1.7 - [1 + 36/Re_\Delta^{*0.75}]^{-1}, \\ \kappa_4^* &= \kappa_3^{\beta_1^* - 1/2}, \\ Re_{\tau\Delta, \text{in}} &= \kappa_4^* (Re_\Delta^*)^{\beta_1^*} [1 + (\kappa_3 Re_\Delta^*)^{-\beta_2^*}]^{(\beta_1^* - 1/2)/\beta_2^*}, \\ \theta &= (1 + Re_\Delta/400)^{-1}, \\ Re_{\tau\Delta}^{\text{com}} &= \theta Re_{\tau\Delta, v} + (1 - \theta) Re_{\tau\Delta, \text{in}}. \end{aligned} \quad (40)$$

To merge with rough-wall representations:

$$Re_{\tau\Delta}^\infty = Re_\Delta \left[\frac{1}{\kappa} \log(\Delta/z_0) + \frac{\chi_x}{2\kappa} (1 - z_0/\Delta) \right]^{-1}, \quad (41)$$

$$Re_{\tau\Delta}^{\text{uf}} = \left[(Re_{\tau\Delta}^{\text{com}})^6 + (Re_{\tau\Delta}^\infty)^6 \right]^{1/6}. \quad (42)$$

References

- [1] Piomelli U. Wall-layer models for large-eddy simulations. *Progress in aerospace sciences*. 2008;44(6):437–446.
- [2] Piomelli U, Balaras E. Wall-layer models for large-eddy simulations. *Annual Rev of Fluid Mech*. 2002;34:349–374.
- [3] Larsson J, Kawai S, Bodart J, et al. Large eddy simulation with modeled wall-stress: recent progress and future directions. *Mechanical Engineering Reviews*. 2016;3(1):15–00418.
- [4] Moeng CH. A large-eddy simulation model for the study of planetary boundary-layer turbulence. *J Atmos Sci*. 1984;6:2311–2330.
- [5] Porté-Agel F, Meneveau C, Parlange MB. A scale-dependent dynamic model for large-eddy simulation: application to a neutral atmospheric boundary layer. *Journal of Fluid Mechanics*. 2000;415:261–284.
- [6] Bou-Zeid E, Meneveau C, Parlange MB. A scale-dependent Lagrangian dynamic model for large eddy simulation of complex turbulent flows. *Phys Fluids*. 2005;17:025105.
- [7] Yang X, Sadique J, Mittal R, et al. Integral wall model for large eddy simulations of wall-bounded turbulent flows. *Physics of Fluids*. 2015;27(2):025112.
- [8] Reichardt H. Vollständige darstellung der turbulenten geschwindigkeitsverteilung in glatten leitungen. *ZAMM-Journal of Applied Mathematics and Mechanics/Zeitschrift für Angewandte Mathematik und Mechanik*. 1951;31(7):208–219.
- [9] Gonzalez DR, Adler MC, Gaitonde DV. Large-eddy simulation of compressible flows with an analytic non-equilibrium wall model. In: *2018 AIAA Aerospace Sciences Meeting*; 2018. p. 0835.
- [10] Adler MC, Gonzalez DR, Riley LP, et al. Wall-modeling strategies for large-eddy simulation of non-equilibrium turbulent boundary layers. In: *AIAA Scitech 2020 Forum*; 2020. p. 1811.
- [11] Kawai S, Larsson J. Wall-modeling in large eddy simulation: Length scales, grid resolution, and accuracy. *Physics of Fluids*. 2012;24(1):015105.
- [12] Bae HJ, Lozano-Durán A, Bose ST, et al. Dynamic slip wall model for large-eddy simulation. *Journal of fluid mechanics*. 2019;859:400–432.
- [13] Lozano-Durán A, Giometto MG, Park GI, et al. Non-equilibrium three-dimensional boundary layers at moderate reynolds numbers. *Journal of Fluid Mechanics*. 2020;883.
- [14] Hinze JO. *Turbulence: An introduction to its mechanism and theory*. McGraw-Hill, New York; 1959.
- [15] Batchelor GK. Pressure fluctuations in isotropic turbulence. *Proc Cambr Phil Soc*. 1951; 47(July 1950):359–374.
- [16] Duprat C, Balarac G, Métais O, et al. A wall-layer model for large-eddy simulations of turbulent flows with/out pressure gradient. *Physics of fluids*. 2011;23(1):015101.
- [17] Nickels T. Inner scaling for wall-bounded flows subject to large pressure gradients. *Journal of Fluid Mechanics*. 2004;521:217–239.
- [18] Jiménez J. Turbulent flows over rough walls. *Annu Rev Fluid Mech*. 2004;36:173–196.